ISSN 0036-0295, Russian Metallurgy (Metally), Vol. 2022, No. 10, pp. 1307–1311. © Pleiades Publishing, Ltd., 2022.
Russian Text © The Author(s), 2022, published in Deformatsiya i Razrushenie Materialov, 2022, No. 4, pp. 13–18.

APPLIED PROBLEMS OF STRENGTH AND PLASTICITY

Role of a Carbon-Fluorine-Containing Additive in the Formation of the Structure, Defect Substructure, and Fracture Surface of an Electric Arc Sprayed Coating

R. E. Kryukov[a], V. E. Gromov[a, *], Yu. F. Ivanov[b], N. A. Kozyrev[a], and Yu. A. Shlyarova[a]
[a] *Siberian State Industrial University, Novokuznetsk, 654006 Russia*
[b] *Institute of High-Current Electronics, Siberian Branch, Russian Academy of Sciences, Tomsk, 634055 Russia*
**e-mail: gromov@physics.sibsiu.ru*
Received October 28, 2021; revised November 15, 2021; accepted December 8, 2021

Abstract—The role of a carbon-fluorine-containing additive in a flux based on the slag of silicomanganese in the formation of the structural-phase state, dislocation substructure, and fracture surface of the coating fabricated by electric arc surfacing using an Sv-08GA wire is analyzed. The relative ferrite and perlite contents and the scalar and excess dislocation densities are quantitatively estimated.

Keywords: electric arc sprayed coating, structure, phase composition, dislocation substructure, flux, additive
DOI: 10.1134/S0036029522100159

INTRODUCTION

An effective method to restore parts and structures subjected to wear and corrosion is to apply coatings on them by surfacing. The required performance properties of such coatings are achieved in the case of using a flux-cored electrode containing carbides, borides, and other high-hardness and high-modulus phases [1]. The increased microhardness and wear resistance of the deposited coatings as compared to the base are due to the formation of a submicro- and nanostructure containing carbide and boride phases, the total fraction of which can reach 40% [2]. A comparative analysis of the structural-phase states and properties of the formed coatings showed that their increased wear resistance is caused by the action of two mechanisms: grain-boundary hardening (in accordance with the Hall–Petch relation) and precipitation hardening. Such coatings are able to withstand abrasive wear and high impact loads [3–8].

Another promising trend in improving the set of physical and mechanical properties of coatings is the modification of the fluxes used in surfacing by the introduction of carbon-containing additives, including the technical waste of metallurgical production [9]. A reasonable choice of a flux material and additives to them for achieving the required level of operational properties of coatings should be based on the results of investigation of the structure, phase composition, dislocation substructure, and fracture of a deposited coating by the methods of modern physical materials science.

The purpose of this work is to study the structural and phase state, the defect substructure, and the fracture surface of coatings deposited under a flux layer with and without a carbon-fluorine-containing additive.

EXPERIMENTAL

7-mm-thick coatings were fabricated by electric arc surfacing using an Sv-08GA wire ((wt %) 0.08% S, <1% Mn) 5 mm in diameter under a flux layer made of the slag of the silicomanganese production with a low manganese oxide content (Table 1) without an additive (hereafter, coating 1) and with a carbon-fluorine-containing FD-UFS additive (see Table 1) in an amount of 6% (hereafter, coating 2). The coatings were deposited onto 16-mm-thick samples made of 09G2S steel ((wt %) 0.09% C, <2% Mn, <1% Si). Surfacing was carried out using an ASAW 1200 weld-

Table 1. Chemical compositions of the flux and an FD-UFS carbon-fluorine-containing additive, wt %

Material	SiO_2	CaO	Al_2O_3	MgO	MnO	FeO	Fe_2O_3	TiO_2	Cr_2O_3	ZnO	C	F	S	P	Al	Na	K	Ca
Flux	35.96	27.99	14.96	8.02	6.69	0.70	–	0.22	0.052	0.013	0.020	0.14	0.64	0.021	–	–	–	–
FD-UFS additive	25.49	–	–	0.13	0.03	–	1.67	–	–	–	13.97	15.06	0.15	0.05	12.28	17.5	12.48	0.74

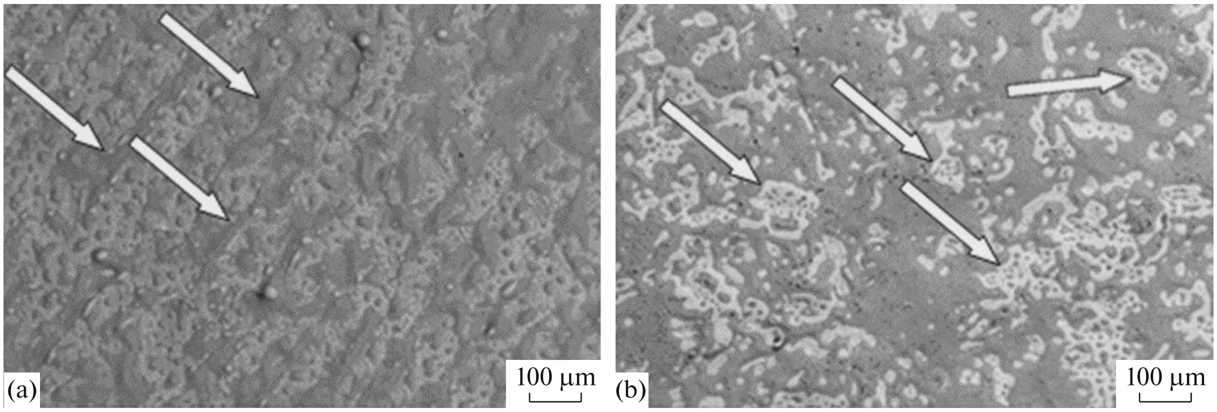

Fig. 1. Surface structure of coating (a) 1 and (b) 2.

ing machine at a current $I = 700$ A, a voltage $U = 30$ V, and a speed v = 30 cm/min. To smooth out the microrelief, the coating surface was processed with a pulsed electron beam on a SOLO installation [10]. The electron beam parameters were as follows: the accelerated electron energy was 17 keV; electron beam energy density, 10 J/cm^2; pulse duration, 50 μs; number of pulses, 3; pulse repetition rate, 0.3 s^{-1}; and residual gas pressure (argon) in the working chamber, 0.02 Pa.

The coating structures were studied by scanning electron microscopy (LEO EVO50, MIRA3 Tesan microscopes) and transmission electron microscopy (JEOL JEM-2100) [11–13]. Samples for transmission electron diffraction microscopy were prepared by electrolytic thinning of plates cut parallel to the substrate surface from the upper part of the coating.

RESULTS AND DISCUSSION

The surface structure of coating 1 has a pronounced ordered structure in the form of bands or layers (indicated by arrows in Fig. 1a). The surface of coating 2 formed under the modified flux has an island-type structure (islands are indicated by arrows in Fig. 1b). The layers and interlayer spaces differ in contrast and structure. The interlayer spaces are fragmented by a network of microcracks (Fig. 2). Cracks are assumed to form along grain boundaries.

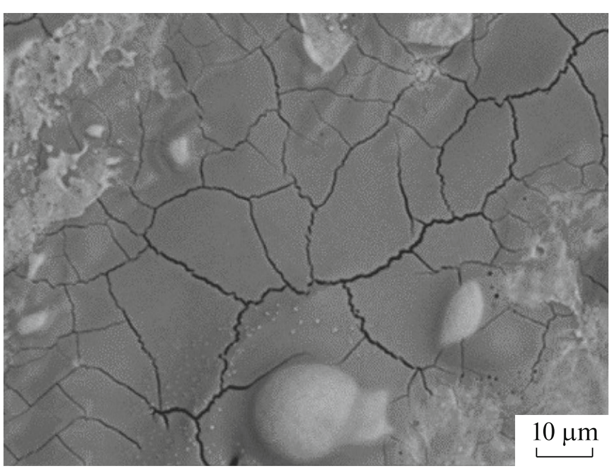

Fig. 2. Structure of the interlayer space in coating 1.

The irradiation of metals and alloys by a pulsed electron beam is known to cause the formation of tensile stresses, the relaxation of which is capable of forming microcracks, in the surface layer [14]. We can assume that the metals of the layers and interlayer spaces differ in the ability to relax the elastic stresses appearing in a coating as a result of high-speed thermal action during irradiation with a pulsed electron beam. The deposited layers are characterized by a relatively more dispersed structure and the absence of microcracks.

SEM studies of the fracture surfaces of the coatings showed that the predominant mechanism of fracture of both coatings is ductile fracture. In this case, a dimple structure characteristic of a ductile fracture forms [15]. Quasi-brittle fracture areas are significantly less frequently detected. This type of fracture is characterized by river-pattern fracture (Fig. 3). Another fracture element of the coatings is represented by micro- and macropores and discontinuities. In coating 1, the number (per unit fracture surface area) of discontinuities and micro- and macropores is greater than in coating 2.

The phases forming the coating metal were identified by indexing electron diffraction patterns and using TEM dark-field images of the microstructure [16, 17]. The results of these studies showed that the main phase is the α phase, i.e., a solid solution based on the bcc iron crystal lattice, regardless of how the coating was formed, with or without a carbon-fluorine-containing additive.

According to the type of defect substructure, α-phase grains can be divided into three types. First,

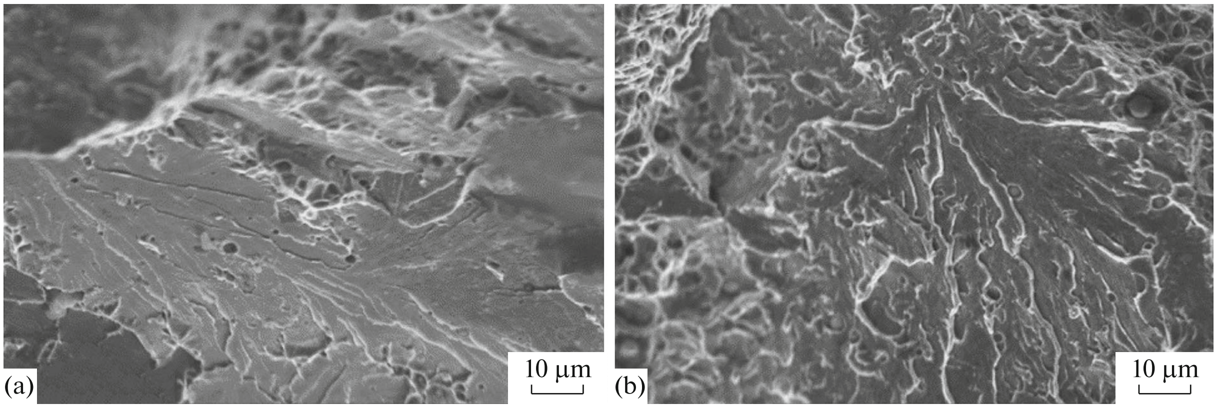

Fig. 3. Structure of the quasi-brittle fracture surface of coating (a) 1 and (b) 2.

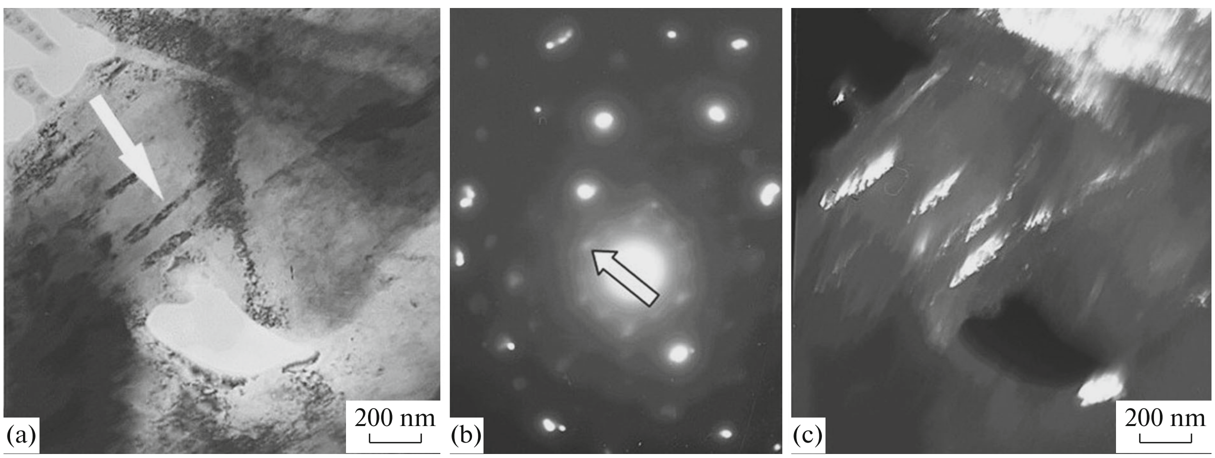

Fig. 4. Pearlitic structure of coating 2: (a) bright field (arrow indicates cementite lamella), (b) electron diffraction pattern, and (c) dark field taken with the $[021]_{Fe_3C}$ reflection. The arrow in (b) indicates the reflection used to form the dark field.

grains, the volume of which contains a subgrain fragmented structure. The fragment sizes change from 150 to 410 nm. The average fragment size is 280 nm in coating 1 and 300 nm in coating 2. An analysis of electron diffraction patterns shows that, in most cases, fragments are separated by low-angle boundaries, the misorientation of which changes within 1–3 deg. Second, there are α-phase grains, the volume of which has no fragments. Third, α-phase grains, the volume of which contains rounded iron carbide (cementite) particles, were detected. The particle sizes change from 20 to 80 nm. Such grains were found only in coating 2.

As noted above, the main volume in both coatings is occupied by ferrite grains: their fraction is 0.85 in coating 1 and 0.55 in coating 2. In both coatings, the main volume of ferrite grains is fragmented: 0.75, in coating 1; 0.3, in coating 2. Along with ferrite grains, lamellar perlite grains were detected, and their characteristic image is shown in Fig. 4. The relative lamellar perlite content in coating 2 is three times higher than in coating 1, 0.45 and 0.15, respectively. This fact is due to the use of a carbon-fluorine-containing additive in coating 2.

A dislocation substructure is present in the volume of grains and fragments (Fig. 5a). Dislocations are randomly distributed or form a network substructure. The structure of the material under study is characterized by elastic stresses [20]. Electron-microscopic images contain bending extinction contours (indicated by arrows in Fig. 5b). The sources of the stress fields are the boundaries of grains, subgrains (fragments), and second-phase inclusions.

Using the generally accepted electron-microscopic methods for analyzing the structure of metals and alloys [18, 19], we determined the scalar (ρ) and excess ($\rho_{\pm}$) dislocation densities and the curvature–torsion amplitude (χ) in a local section in the foil metal (Table 2).

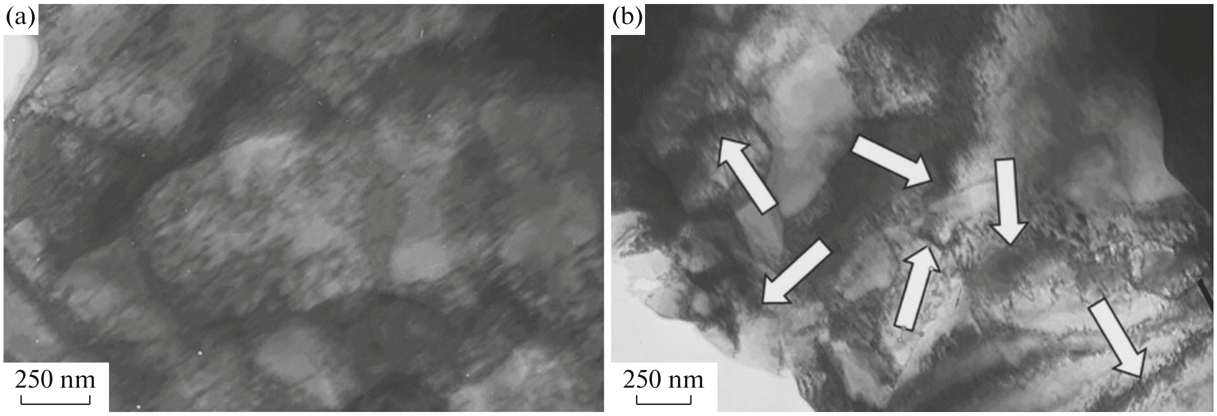

Fig. 5. Dislocation substructure of the coatings.

The scalar dislocation density ρ averaged over all structural components of the material in coating 2 is 1.24 times higher than in coating 1. The largest value of ρ in coating 1 was found in perlite grains, and that in coating 2, in unfragmented ferrite grains. The excess dislocation density $\rho_{\pm}$ is also higher in coating 2: 1.32 times compared to coating 1. In both coatings, the highest scalar and excess dislocation densities are detected in unfragmented ferrite grains, and their lowest values are in fragmented ferrite grains. Obviously, this is due to the restructuring of the dislocation substructure and the departure of some dislocations into low-angle fragment boundaries.

The bending-torsion amplitude (proportional to the internal long-range stress fields) in coating 2 is 3.8 times higher than in coating 1. The most stressed state is characteristic of unfragmented ferrite grains in coating 1 and of fragmented ferrite grains in coating 2.

CONCLUSIONS

(1) The coatings fabricated by surfacing using an Sv-08GA wire under a layer of the flux made of the slag of the silicomanganese production have a layered structure, and those in the case of modifying the flux with a carbon–fluorine-containing FD-UFS additive have an insular structure.

(2) The predominant mechanism of fracture of the coatings of both types is ductile fracture.

(3) The main structural component of both types of coatings is represented by α-iron grains; in most cases α-phase grains are fragmented.

(4) The modification of the flux with the carbon-fluorine-containing additive leads to a threefold increase in the fraction of lamellar perlite in the coating.

(5) The coating fabricated under the modified flux is characterized by a higher dislocation density (scalar, excess) and a higher curvature–torsion amplitude.

Table 2. Characteristics of the defect substructure of sprayed coatings 1 and 2

Parameter	Pearlite		Unfragmented ferrite		Fragmented ferrite		Ferrite–carbide mixture		On average over material	
	no. 1	no. 2	no. 1	no. 2	no. 1	no. 2	no. 1	no. 2	no. 1	no. 2
Volume fraction	0.15	0.45	0.1	0.15	0.75	0.3	No	0.1		
ρ, 10^{10}, cm^{-2}	3.23	2.79	2.35	3.32	1.75	1.47	No	3.23	2.03	2.52
$\rho_{\pm}$, 10^{10}, cm^{-2}	1.94	2.8	2.02	3.22	1.74	1.32	No	2.42	1.8	2.38
χ, cm^{-1}	485	700	505	805	435	3290	No	2880	450	1710

CONFLICT OF INTEREST

The authors declare that they have no conflicts of interest.

REFERENCES

1. E. V. Kapralov, S. V. Raikov, E. A. Budovskikh, V. E. Gromov, E. S. Vashchuk, and Yu. F. Ivanov, "Structure, phase composition, and properties of surfacing formed on steel by electric arc method," Fundam. Probl. Sovr. Materialoved. **11** (3), 334–339 (2014).
2. V. E. Gromov, E. V. Kapralov, S. V. Raikov, Yu. F. Ivanov, and E. A. Budovskikh, "Structure and properties of wear-resistant coatings deposited by the electric arc method on steel with flux-cored electrodes," Usp. Fiz. Met. **15**, 211–232 (2014).
3. R. Li, D. Y. He, Z. Zhou, Z. J. Wang, and X. Y. Song, "Wear and high temperature oxidation behavior of wire arc sprayed iron based coatings," Surf. Eng. **30**, 784–790 (2014).
4. R. Kejžar and J. Grum, "Hardfacing of wear-resistant deposits by MAG welding with a flux-cored wire having graphite in its filling," Weld. Int. **20**, 961–976 (2005).
5. H. R. Ma, X. Y. Chen, J. W. Li, C. T. Chang, G. Wang, H. Li, X. M. Wang, and R. W. Li, "Fe-based amorphous coating with high corrosion and wear resistance," Surf. Eng. **46**, 1–7 (2016).
6. Yu. Zhuk, "Super-hard wear-resistant coating systems," Mater. Technol. **14**, 126–129 (1999).
7. M. Kirchgabner, E. Badisch, and F. Franek, "Behaviour of iron-based hard facing alloys under abrasion and impact," Wear **265**, 772–779 (2008).
8. N. A. Kozyrev, A. I. Gusev, R. E. Kryukov, A. A. Usol'tsev, and L. P. Baschenko, "Development of new flux-cored electrodes for surfacing. Flux-cored electrode for surfacing of the parts working under shock-abrasive wear conditions," Chern. Metall. Byul. Nach.-Tekh. Ekonom. Inf., No. 7, 70–77 (2018).
9. N. A. Kozyrev, R. E. Kryukov, N. E. Kryukov, A. A. Usol'tsev, and A. R. Mikhno, "Development of new welding fluxes using carbon-fluorinated additives," Teoriya Tekhnol. Metall. Proizv., No. 3(26), 17–25 (2018).
10. *Electron-Ion-Plasma Modification of the Surfaces of Nonferrous Metals and Alloys*, Ed. by N. N. Koval and Yu. F. Ivanov (NTL, Tomsk, 2016).
11. F. R. Egerton, *Physical Principles of Electron Microscopy* (Springer Int. Publ., Basel, 2016).
12. C. S. S. R. Kumar, *Transmission Electron Microscopy. Characterization of Nanomaterials* (Springer, New York, 2014).
13. C. B. Carter and D. B. Williams, *Transmission Electron Microscopy* (Springer Int. Publ., Berlin, 2016).
14. V. P. Rotshtein, D. I. Proskurovskii, and G. E. Ozur, *Modification of the Surface Layers of Metallic Materials by Low-Energy High-Current Electron Beams* (Nauka, Novosibirsk, 2019).
15. *Fractography and Atlas of Fractographs: A Handbook* (Metallurgiya, Moscow, 1982).
16. L. M. Utevskii, *Diffraction Electron Microscopy in Metal Science* (Metallurgiya, Moscow, 1973).
17. K. Andrews, D. Dyson, and S. Keown, *Interpretation of Electron Diffraction Patterns* (Macmillan, London, 1968).
18. K. S. Chernyavskii, *Stereology in Metal Science* (Metallurgiya, Moscow, 1977).
19. N. A. Koneva, E. V. Kozlov, L. I. Trishkina, and D. V. Lychagin, "Long-range stress fields, curvature–torsion of a crystal lattice, and the stages of plastic deformation. Measurement methods and results," in *Proceedings of International Conference on New Methods in Physics and Mechanics of Deformable Solids* (TGU, Tomsk, 1990), pp. 83–93.
20. P. Hirsch, A. Howie, R. Nicholson, D. Pashley, and M. Whelan, *Electron Microscopy of Thin Crystals* (Plenum, New York, 1967).

Translated by K. Shakhlevich